Measuring Bubble, Drop and Particle Sizes in Multiphase Systems with Ultrasound

A. H. G. Cents, D. W. F. Brilman, and G. F. Versteeg
Dept. of Chemical Engineering, University of Twente,
P.O. Box 217, 7500 AE Enschede, The Netherlands

P. J. Wijnstra and P. P. L. Regtien
Dept. of Electrical Engineering, University of Twente,
P.O. Box 217, 7500 AE Enschede, The Netherlands

DOI 10.1002/aic.10203
Published online in Wiley InterScience (www.interscience.wiley.com).

A technique is developed for measurement of bubble, droplet and particle-size distributions in multiphase systems, based on the propagation speed and attenuation of ultrasound. The measurement of the size distribution of the dispersed phase in multiphase systems was desired to analyze the mass-transfer mechanism in gas-liquid-liquid and gas-liquid-solid systems. To obtain this information, both the ultrasonic velocity and the attenuation coefficient of tone-burst signals are determined for a large frequency range (typically 100 kHz – 100 MHz). From these parameters, the size distributions and the volume fraction of the different dispersed phases can be determined using a scattering model. It was shown that the interfacial area can be determined very accurately, however, for the exact size distribution of the gas bubbles in the used size range (1–3 mm) an independent gas holdup determination is required. Experiments were performed in gas-liquid, solid-liquid, and gas-liquid-solid systems. The results showed good agreement of the particle-size distribution compared to a commercial laser-scattering analyzer, both with and without gas bubbles present. Furthermore, a good agreement between the scattering model and the experiments was found in the systems that contained gas bubbles, but these results should be validated using for instance, a digital camera technique.
 AIChE J, 50: 2750–2762, 2004
Keywords: ultrasound, multiphase, size distribution, mass transfer

Introduction

In chemical engineering the rate of mass transfer between two different phases often directly determines the production rate of the process (for example, the gas absorption rate in gas-liquid systems). This mass-transfer rate is proportional to both a mass-transfer coefficient, as well as the specific interfacial area between the different phases. Both parameters depend mainly on the (local) hydrodynamic situation inside the system. For both design purposes and for improvement of existing production facilities, it is very important to be able to analyze and to predict these parameters.

Especially for three-phase systems, the prediction of the gas-liquid mass- transfer rate is rather difficult as the interaction between dispersed phase particles, which can be either solid particles or liquid phase droplets of an immiscible phase, is not yet understood. In literature (Yoshida et al., 1970) both enhancements, as well as retardations of mass-transfer (gas absorption) rates on the addition of a dispersed phase, are reported. Recent investigations (Cents et al., 2001) have shown

Correspondence concerning this article should be addressed to A. H. G. Cents at toine.cents@sasol.com.

that for some specific systems the enhancement of mass transfer in stirred vessels could be well described by the so-called shuttle-mechanism, which assumes dispersed phase droplets to be present in the mass- transfer zone, thereby facilitating mass transfer due to their higher solubility for the gaseous component to be transferred. However, some other dispersed phases, also having a higher solubility for the gas, did not enhance the mass- transfer rate. Therefore, a conclusive understanding of this phenomenon does not yet exist.

A possible correlation may exist with the size of the dispersed droplets, which can influence the liquid-liquid mass transfer, and can also play a role in the attraction of the droplets to the gas-liquid interface. For this reason, it is important to develop a technique, which can measure the bubble-size distribution (from which the Sauter mean diameter can be calculated) and the gas volume fraction, as well as the size distribution of the dispersed droplets, simultaneously. The bubble-size distribution and gas holdup are very important in gas-liquid mass transfer, because they determine the specific interfacial area. The determination of the droplet-size distribution is necessary to improve on the insight in the mechanisms of mass transfer in gas-liquid-liquid (G-L-L) and gas-liquid-solid (G-L-S) systems.

Characterization of size distributions and phase volume fractions is a recognized problem in chemical engineering. The specific gas-liquid interfacial area is usually determined using a light scattering technique (Calderbank, 1958; Calderbank et al., 1960), or by simultaneous determination of the gas holdup and the bubble-size distribution. Methods to determine the bubble diameter include photography (with digital image analysis) (Machon et al., 1997; Pacek et al., 1994) and capillary techniques with light transmission analysis (Barigou and Greaves, 1991; Bae and Tavlarides, 1989) or by using contact probes (Burgess and Calderbank, 1975; Calderbank and Pereira, 1977). However, all these techniques have limited applicability, because they only allow for small volume fractions and require transparent solutions. Capillary techniques can also be inaccurate, because of possible coalescence and breakup of bubbles inside the sampling probe, and difficulties related to isokinetic sampling. Also, the presence of small droplets or particles in G-L-L or G-L-S systems often interferes with the traditional measurement techniques, and it is definitely not possible to measure the size distribution of the additional liquid or solid phase in this way.

In this work, a technique has been developed, which can simultaneously determine the size distributions of *both* dispersed phases in G-L-L or G-L-S systems using ultrasonic spectroscopy. The measurement principle of this technique is the dependence of ultrasonic velocity and attenuation on particle size and dispersed phase holdup, and this varies with frequency.

In the past some work was done on the determination of particle sizes in two-phase systems with ultrasonic spectroscopy. Bubble-size distribution determination with ultrasound has been used in oceanographic applications for measurement of small bubble sizes near their resonance frequency (Medwin, 1977). Stravs and Von Stockar (1985) and Stravs et al. (1986) used high- frequency (1–10 MHz) ultrasound for on-line monitoring of the interfacial area in fermentation bubble columns. These authors were able to measure interfacial areas up to 350 m^{-1} in their setup, but did not determine bubble-size distributions. An ultrasonic pulse technique was used by McClements and Fairley (1991) and McClements (1996) for the determination of droplet-size distributions in stabilized liquid-liquid emulsions. In this work, velocity and attenuation measurements of the ultrasonic waves were performed in order to measure small (<1 μm) droplets. For the characterization of solid particle-size distributions, both the attenuation coefficient, as well as the velocity of ultrasonic waves were used by Khatchikian et al. (1999). These authors, who used glass beads of 24–485 μm, obtained a good agreement with the theory for scattering of ultrasound by particles.

In this work, an ultrasonic measurement system is developed, which can measure bubble, droplet, and particle-size distributions in multiphase systems. Due to the broad range of frequencies used (100 kHz – 100 MHz), particle sizes from 1 μm to approximately 1 cm can be determined. The technique is able to measure the volume fractions and the size distributions, because it makes use of both the velocity of sound, as well as the attenuation coefficient at the used frequency band. Both these profiles contain useful information for *in situ* determination of the important characteristics of three-phase systems.

Theory

General theory

The theory of ultrasonic propagation in multiphase systems is based on mathematical treatment of the behavior of an incoming ultrasonic wave in a fluid containing an ensemble of particles. The ultrasonic velocity and attenuation coefficient of a multiphase system are directly related to the physical properties of the individual phases, and also depend on the size and volume fraction of the particles, as well as on the frequency of the transmitted wave. As the wave travels through the liquid, the velocity and the amplitude of the wave are changed due to the interaction with the particles that are present in the fluid. Several mechanisms can account for the alteration of the incoming wave (McClements, 1996):

(1) Scattering of the wave into directions that are different from that of the incoming wave.

(2) Conversion of ultrasonic energy into heat due to various absorption mechanisms.

(3) Interference of the waves, which travel through a particle with waves that travel only in the continuous phase and with scattered waves.

The full ultrasonic theory to describe these phenomena was first derived by Epstein and Carhart (1953). They investigated the attenuation of sound in fogs, so their analysis was based on liquid drops in air. Allegra and Hawley (1972) modified the stress tensor of a viscous fluid into that of an elastic solid to obtain the wave equations for a system of solid particles in a liquid. Together, these two theories are commonly referred to as the ECAH-theory.

The basis of this theory is the linearization of the equations for conservation of mass, momentum, and energy. Together with a thermal and a caloric equation of state, relating the density and internal energy to pressure and temperature, the equations can be rewritten to obtain the following set of acoustic wave equations

$$(\nabla^2 + k_c^2)\phi_c = 0 \tag{1}$$

$$(\nabla^2 + k_T^2)\phi_T = 0 \tag{2}$$

$$(\nabla^2 + k_s^2)\mathbf{A} = 0 \tag{3}$$

with the propagation constants

$$k_c = \omega/c + i\alpha \quad \text{(compressional wave)} \tag{4}$$

$$k_T = (1 + i)\sqrt{\omega/2\sigma} \quad \text{(thermal wave)} \tag{5}$$

$$k_s = (1 + i)\sqrt{\omega/2\nu} \quad \text{(shear wave)} \tag{6}$$

Using these equations, the problem of a plane wave encountering a sphere suspended in a liquid can be solved using spherical co-ordinates. The sphere gives rise to a reflected compressional wave, a compressional wave inside the sphere and thermal and shear waves inside and outside the sphere. The solution of the wave equations consists of series expansions of spherical Bessel functions and spherical harmonics with six unknown scattering coefficients (A_n, B_n, C_n, A'_n, B'_n, and C'_n). In order to solve the complete acoustic field, these coefficients need to be determined using six boundary conditions: continuity of temperature, heat flux, radial, and tangential stress and radial and tangential velocity at the surface of the particle. When these boundary conditions are applied, the following set of six linear equations result, from which the six unknown scattering coefficients can be determined.

Continuity of Radial Velocity

$$a_c j'_n(a_c) + A_n a_c h'_n(a_c) + B_n a_T h'_n(a_T) - C_n n(n+1) h_n(a_s) = A'_n a'_c j'_n(a'_c) + B'_n a'_T j'_n(a'_T) - C'_n n(n+1) j_n(a'_s) \tag{7a}$$

Continuity of Tangential Velocity

$$j_n(a_c) + A_n h_n(a_c) + B_n h_n(a_T) - C_n(h_n(a_s) + a_s h'_n(a_s)) = A'_n j_n(a'_c) + B'_n j_n(a'_T) - C'_n(j_n(a'_s) + a'_s j'_n(a'_s)) \tag{7b}$$

Continuity of Temperature

$$b_c(j_n(a_c) + A_n h_n(a_c)) + B_n b_T h_n(a_T) = A'_n b'_c j_n(a'_c) + B'_n b'_T j_n(a'_T) \tag{7c}$$

Continuity of Heat Flux

$$\tau(a_c b_c(j'_n(a_c) + A_n h'_n(a_c)) + B_n b_T a_T h'_n(a_T)) = \tau'(A'_n b'_c a'_c j'_n(a'_c) + B'_n b'_T a'_T j'_n(a'_T)) \tag{7d}$$

Continuity of Radial Stress

$$\eta\begin{Bmatrix}[(a_s^2 - 2a_c^2) j_n(a_c) - 2a_c^2 j''_n(a_c)] + \\ A_n[(a_s^2 - 2a_c^2) h_n(a_c) - 2a_c^2 h''_n(a_c)] + \\ B_n[(a_s^2 - 2a_T^2) h_n(a_T) - 2a_T^2 h''_n(a_T)] + \\ 2n(n+1) C_n[a_s h'_n(a_s) - h_n(a_s)]\end{Bmatrix} = \eta'\begin{Bmatrix}A'_n[(a'^2_s - 2a'^2_c) j_n(a'_c) - 2a'^2_c j''_n(a'_c)] + \\ B'_n[(a'^2_s - 2a'^2_T) j_n(a'_T) - 2a'^2_T j''_n(a'_T)] + \\ 2n(n+1) C'_n[a'_s j'_n(a'_s) - j_n(a'_s)]\end{Bmatrix} \tag{7e}$$

Continuity of Tangential Stress

$$\eta\begin{Bmatrix}a_c j'_n(a_c) - j_n(a_c) + A_n[a_c h'_n(a_c) - h_n(a_c)] + \\ B_n[a_T h'_n(a_T) - h_n(a_T)] - \\ 1/2 C_n[a_s^2 h''_n(a_s) + (n^2 + n - 2) h_n(a_s)]\end{Bmatrix} = \eta'\begin{Bmatrix}A'_n[a'_c j'_n(a'_c) - j_n(a'_c)] + B'_n[a'_T j'_n(a'_T) - j_n(a'_T)] \\ - 1/2 C'_n[a'^2_s j''_n(a'_s) + (n^2 + n - 2) j_n(a'_s)]\end{Bmatrix} \tag{7f}$$

In the equations, the following notation is used: j_n and h_n are spherical Bessel functions of order n, and spherical Hankel functions of the first-kind and order n, respectively. Primed functions are first or second derivatives of these functions. $a_c = k_c r$, $a_T = k_T r$ and $a_s = k_s r$. For primed and unprimed quantities, the following abbreviations are used

$$b_c = \frac{(1 - \gamma)\omega^2}{\beta c^2} \tag{8}$$

$$b_T = \frac{i\omega}{\beta\sigma} = i\omega\frac{\rho C_p}{\beta\tau} \tag{9}$$

$$\gamma = 1 + \frac{T\beta^2 c^2}{C_p} \tag{10}$$

When $n = 0$, Eq. 7b and 7f are not valid and all terms containing C_n and C'_n vanish from the remaining equations. Now a system with four equations (7a, 7c, 7d, and 7e) and four unknowns (A_n, A'_n, B_n and B'_n) has to be solved.

In case of a solid as the dispersed phase, the viscosity (η') in Eqs. 6, 7e, and 7f has to be replaced with $\mu'/(-i\omega)$, where μ' is the shear rigidity of the solid. For b'_T, the following relation then has to be applied

$$b'_T = \frac{\gamma}{c_1^2\beta}\left[\omega^2 - \left(\frac{c_1^2}{\gamma} - \frac{4i\omega\mu}{3\rho}\right)\frac{i\omega}{\sigma}\right] \tag{11}$$

In this equation c_1 is the speed of sound for spherical compressional waves in an elastic isotropic solid.

Relationship between the scattering coefficient and velocity and attenuation

In the previous section the complete ultrasonic field around a single particle was described with the ultrasonic theory. It is important to relate the calculated scattering coefficient of the compressional wave in the continuous phase (A_n) into measurable quantities: the ultrasonic velocity (c), and the attenuation coefficient (α). These quantities are contained in the complex propagation constant K, which is defined as

$$K = \omega/c + i\alpha \tag{12}$$

In dilute systems the scattering and absorption of a wave encountering a particle is not influenced by the neighboring particles. The complex propagation constant is then calculated as (Foldy, 1945)

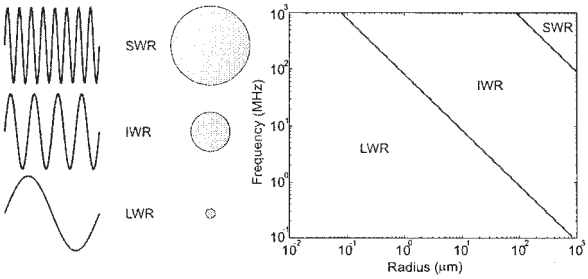

Figure 1. Different regimes for interaction of ultrasonic waves with particles (following McClements, 1996).

$$\left(\frac{K}{k_{c1}}\right)^2 = 1 + \frac{4\pi N f(0)}{k_{c1}^2} \tag{13}$$

In more concentrated systems interaction between the particles becomes significant. In these systems multiple scattering has to be taken into account. A comprehensive and widely used relation is the one proposed by Waterman and Truell (1961)

$$\left(\frac{K}{k_{c1}}\right)^2 = 1 + \frac{4\pi N f(0)}{k_{c1}^2} + \frac{4\pi^2 N^2}{k_{c1}^4}\left(f(0)^2 - f(\pi)^2\right) \tag{14}$$

In Eqs. 13 and 14, N is the number density of the particles ($N = 3\varepsilon/4\pi r^3$), and $f(0)$ and $f(\pi)$ are the so-called far-field scattering amplitudes that are defined as

$$f(0) = \frac{1}{ik_{c1}} \sum_{n=0}^{\infty} (2n+1) A_n \tag{15}$$

$$f(\pi) = \frac{1}{ik_{c1}} \sum_{n=0}^{\infty} (-1)^n (2n+1) A_n \tag{16}$$

Size distributions

Bubbles, drops, and particles in multiphase systems are usually not monosize, but have a certain size distribution. The most practical way to determine the velocity, and the attenuation coefficient in such a system, is to make use of superposition of discrete particle size classes. The Waterman Truell (Eq. 14) applied to distributions then becomes

$$\left(\frac{K}{k_{c1}}\right)^2 = 1 + \frac{4\pi}{k_{c1}^2} \sum_j N_j f_j(0) + \frac{4\pi^2}{k_{c1}^4} \sum_j N_j^2 \left(f_j(0)^2 - f_j(\pi)^2\right) \tag{17}$$

in which index j corresponds to the discrete size class j.

Simplified interaction regimes

To get a better understanding of the mechanisms that can account for the change of the incoming wave, it is convenient to divide the interaction between the ultrasonic wave, and the particle into three regimes (Figure 1).

(1) The long wavelength regime (LWR): $r \ll \lambda$
(2) The intermediate wavelength regime (IWR): $r \sim \lambda$
(3) The short wavelength regime (SWR): $r \gg \lambda$

In this work measurements in the LWR, as well as the IWR, are performed. The SWR is not reached and will, therefore, not be discussed. In the LWR three types of interactions are of importance: intrinsic absorption, particle pulsation, and particle oscillation. The intrinsic absorption is equal to the sum of the absorption of acoustic energy in the continuous and dispersed phases, and depends on their volume fractions and *not* on the size of the particles. The pulsation of particles occurs due to the difference in compressibility and/or difference in thermal properties between the particle, and the surrounding continuous phase. The pulsation of the particle leads to scattering of the ultrasonic wave in all directions (monopole scattering), and the conversion of ultrasonic energy into heat (thermal absorption). Particle oscillations occur due to a density difference between the particle and the surrounding fluid. The particle moves forward and backward because its inertia differs from the continuous phase. A part of the incoming wave is scattered away (dipole scattering) and part of the ultrasonic energy is converted into heat (visco-inertial absorption), due to the damping of the particle movement, because of viscous drag.

In the IWR the interactions between the particle and the ultrasonic wave are much more complex. For gas-liquid (G-L) and liquid-liquid systems (L-L), the scattering of the waves is dominant over other types of interaction. Because of the complicated interactions, much higher orders of scattering have to be taken into account. The scattering coefficients can be calculated from the following equation, which can be derived from Eqs. 7b and 7e, neglecting thermal and shear waves and terms that do not contribute significantly in Eq. 7e

$$A_n = \frac{\rho_1 a_c' j_n(a_c) j_n'(a_c') - \rho_2 a_c j_n(a_c') j_n'(a_c)}{\rho_2 a_c j_n(a_c') h_n'(a_c) - \rho_1 a_c' j_n'(a_c') h_n(a_c)} \tag{18}$$

where $a_c = k_c \cdot r$, and where j_n are spherical Bessel functions, and h_n are spherical Hankel functions of the first-kind. Primed quantities are derivatives of the spherical harmonics. This result was also obtained by Gaunaurd and Überall (1981). The results for the ultrasonic velocity and the attenuation coefficient in G-L systems were also compared to the theory of Nishi (1975). The results of both theories are in complete agreement for bubbles in the range of 0.5 – 20 mm in diameter, which are discussed in this work.

In solid-liquid (S-L) systems viscous forces are important and always have to be taken into account. Thermal waves are relatively unimportant in these systems and can, therefore, be neglected. For measurements that are completely in either the LWR or the IWR simplified solutions can be used. Otherwise, the complete ultrasonic theory has to be applied.

Three-phase systems

In the case of three-phase systems (G-L-S or G-L-L) two different types of dispersed phase particles (gas bubbles, and solid particles, or gas bubbles and liquid droplets), each having its own size distribution, will influence the propagation of sound through the medium. In dilute systems, these size distributions can be determined by superposition of the two

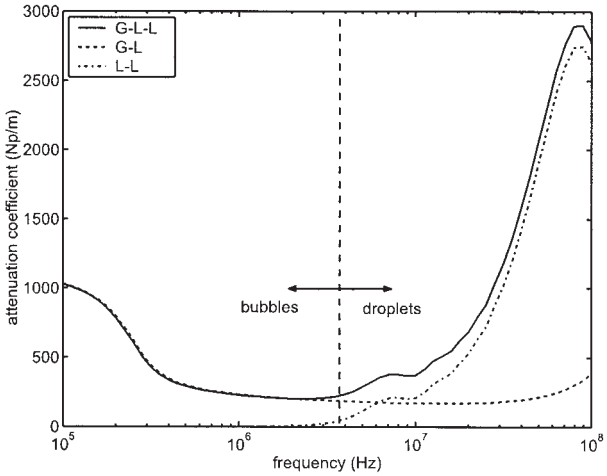

Figure 2. Attenuation coefficient of a G-L-L system with 10% air bubbles of 1 mm and 10% hexadecane droplets of 100μm in water.

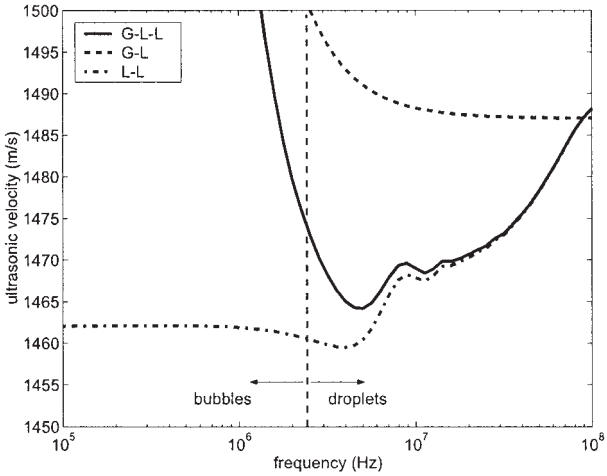

Figure 4. Zoom of the ultrasonic velocity of a G-L-L system with 10% air bubbles of 1 mm and 10% hexadecane droplets of 100 μm in water (Note the scale).

phases. In nondilute systems interactions between the particles are important. The complex propagation constant K can be calculated using Eq. 17, including both phases in the summation. In Figures 2 and 3 the attenuation and velocity coefficient in a G-L-L system are presented.

From these figures, it can be concluded that characteristic profiles from both phases are retained in both the velocity, as well as in the attenuation coefficient profile. From Figure 2, it can be seen that the attenuation due to the gas bubbles of the order of millimeters is most strong in the lower-frequency domain ($<$ 1MHz). The droplets, which are typically in the range of a few hundred micron or smaller, attenuate in the higher-frequency domain. This type of behavior is also present in the velocity profile, but on a different scale. From Figure 3, it seems that the velocity is only changed by the presence of the gas bubbles. However, in Figure 4 the effect of the droplets on velocity is very clear.

The attenuation coefficient and to a lesser extent the velocity

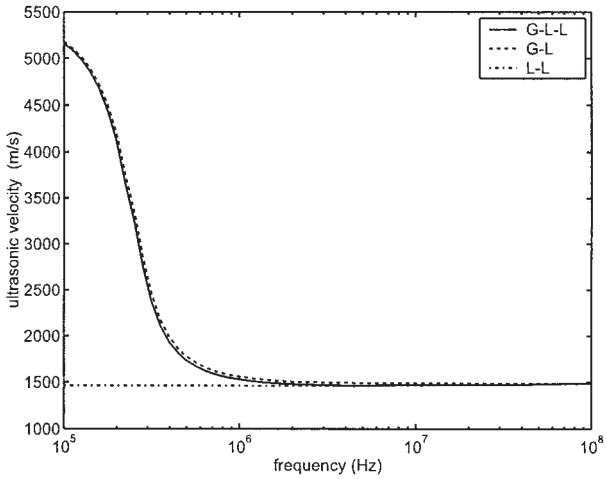

Figure 3. Ultrasonic velocity of a G-L-L system with 10% air bubbles of 1 mm and 10% hexadecane droplets of 100μm in water.

are very useful in the determination of the broadness of the size distributions. Strong effects, due to the resonance of particles with a certain size, are damped due to the presence of particles with a different diameter, which have a different resonance frequency. From the smoothness of both profiles, the variance of the distribution can be determined.

When both the attenuation coefficient as well as the velocity are measured sufficiently accurately, it is possible to extract the size distributions for both phases from the experiments.

The inverse problem

In the previous section it was explained how to determine the velocity and the attenuation coefficient using the ECAH-theory when the size distributions and the dispersed phase holdup are known. The actual problem is opposite: the derivation of the size distributions and the volume fractions of the different dispersed phases from the experimental values of the velocity, and the attenuation coefficient, respectively. Ideally, it would be desirable to solve this problem without making any assumption on the size distribution (Spelt et al., 1999; Duraiswami et al., 1998). However, this is more laborious and increases the sensitivity to experimental errors significantly. Therefore, in this work the size distribution type (normal, log-normal, and so on) is preselected. An advantage of using a model distribution is that only two or three parameters (depending on the distribution) have to be optimized. In chemical engineering applications the dispersed phase size distribution can often be described satisfactorily accurate using a log-normal distribution in case of gas bubbles and liquid droplets. Of course, it is important to verify whether the assumption of a distribution influences the results significantly using different distributions. The log-normal distribution is described by

$$P(x) = \frac{1}{Sx\sqrt{2\pi}} \exp\left(-\frac{(\ln(x) - M)^2}{2S^2}\right) \qquad (19)$$

The mean diameter and variance can be calculated from this distribution

$$\mu = \exp(M + \tfrac{1}{2}S^2) \tag{20}$$

$$\sigma = \exp(S^2 + 2M) \cdot (\exp(S^2) - 1) \tag{21}$$

The Sauter mean diameter for an arbitrary distribution is defined as

$$d_{32} = \frac{\sum_i N_i d_i^3}{\sum_i N_i d_i^2} \tag{22}$$

The best fit between the experiments and the model is determined by minimizing the sum of the squares of both the velocity and the attenuation measurements. As an objective function for this minimization, the following equation is proposed

$$f = y \sum_i (c_E(i) - c_M(i))^2 + (1 - y) \sum_i (\alpha_E(i) - \alpha_M(i))^2 \tag{23}$$

Depending on the absolute values of the velocity and the attenuation coefficient, a suitable coefficient y can be chosen.

Alternative determination of volume fraction

In order to determine the important value for the specific interfacial area (a) between different phases, not only the size distribution of the particles, but also their volume fraction ε, must be known. This area can be determined from

$$a = \frac{6 \cdot \varepsilon}{d_{32}} \tag{24}$$

For solid-liquid (S-L) and liquid-liquid (L-L) systems, determination of the volume fraction from the ultrasonic velocity and attenuation coefficient measurements is relatively simple, because the frequency dependent profiles are very characteristic to both particle diameter, as well as volume fraction. The effect of volume fraction and particle diameter on ultrasonic velocity in L-L systems is shown in Figure 5.

From Figure 5, it can be seen that it is possible to extract the volume fraction of the dispersed phase from the velocity measurements at the lower frequencies. The mean diameter d_{32} can be determined from the position of the positive slope in this measurement. The absolute values for these changes depend on the physical properties of both phases.

In gas-liquid (G-L) systems, however, the profiles are much less characteristic and problems can arise with simultaneous determination of d_{32} and ε. In Figure 6a this problem is visualized. When bubbles are in the range of millimeters, the velocity vs. frequency profile has an exponentially decreasing shape. The shift of the profile due to a change in volume fraction is vertical, and the shift due to a change in bubble diameter is horizontal. This results in an overlap, where it is possible to have multiple solutions (that is, different combinations of bubble size and gas holdup leading to the same profiles) for a single set of experiments. The attenuation coefficient cannot be used to discriminate between a broad-size distribution and a monosize bubble distribution. This phenomenon is also depicted in Figure 6. An advantage of the method is that the interfacial area, calculated using Eq. 24, can be determined very accurately from the profiles, which is, in fact, the most important parameter in many applications.

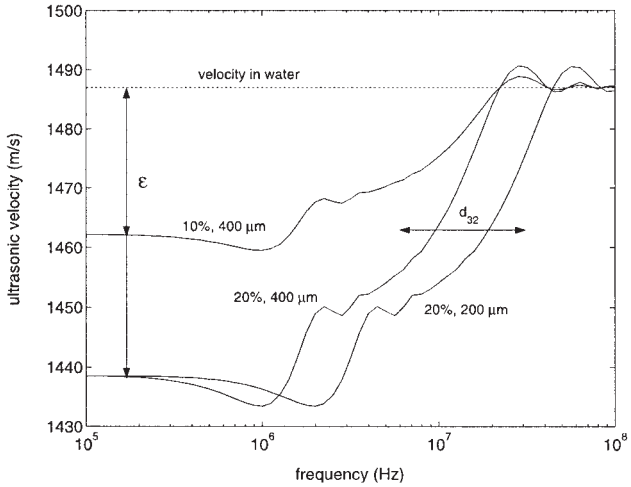

Figure 5. Ultrasonic velocity in a L-L system with different size and volume fractions of hexadecane droplets.

In case both the size distribution, as well as the volume fraction, respectively, have to be determined independently, an alternative measurement of the gas holdup is necessary. A relatively simple and accurate method is to make use of electrical conductivity, which was applied among others by Yianatos et al. (1985). The electrical conductivity of an aqueous medium is changed by the presence of nonconducting particles, droplets, or bubbles. The conductivity of the medium is proportional to the effective cross-sectional area of the bubbles, and inversely proportional to the effective path length between the electrodes

$$G = 1/R \sim A/L \tag{25}$$

The dimensionless conductivity of the medium is defined as the ratio of the conductivity of the dispersion to the continuous phase and is given by

$$\gamma = \frac{G_\varepsilon}{G} = \frac{A_\varepsilon/A}{L_\varepsilon/L} \tag{26}$$

where

$$A_\varepsilon = A(1 - \varepsilon) \tag{27}$$

$$L_\varepsilon = \xi L \tag{28}$$

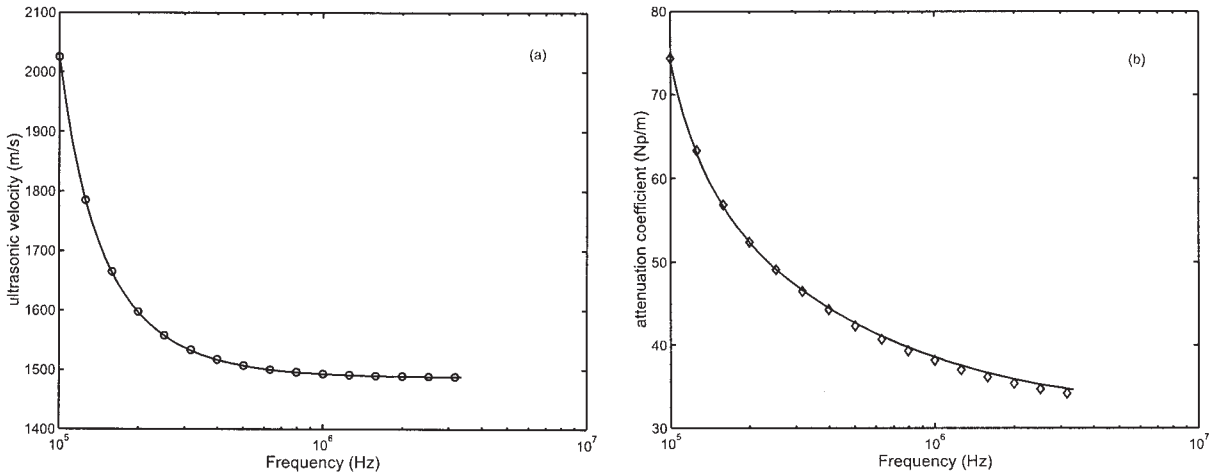

Figure 6. Multiple solutions for gas-liquid systems with different gas fraction and Sauter mean diameter.

Open symbols: $\varepsilon = 6.0\%$, $\mu = 3.00$ mm, $\sigma = 0$ mm (monosize), $d_{32} = 3.00$ mm and $a = 120.2$ m^2/m^3 closed lines: $\varepsilon = 6.5\%$, $\mu = 2.78$ mm, $\sigma = 0.75$ mm, $d_{32} = 3.23$ mm and $a = 120.9$ m^2/m^3.

In Equation 28 ξ is the tortuosity for which different models are developed. The model of Weissberg (1963) holds in bubbly zones (0–30% gas holdup), and in froth zones (65–90% gas holdup)

$$\xi = 1 - 0.5 \ln(1 - \varepsilon) \tag{29}$$

In the experiments in this work the gas holdup never exceeds 20%. In this range the different models for the tortuosity do not differ significantly. From measurements of the ratio of the conductivity in the dispersion and the continuous fluid, it is possible to determine the gas holdup using Eqs. 25–29.

When a nonpolar solvent is used as the continuous phase, this technique cannot be applied due to the absence of electrical conductivity in the continuous phase, and the local gas holdup should be determined using an alternative technique (for instance, with a fiber optic probe).

Measurement Method

Setup

The experimental setup consists of an arbitrary waveform generator (AWG), which sends any desired electric signal to a piezo-electric transducer (T). The signal is amplified with a maximum of 44 dB, with a variable power amplifier. The transmitting transducer converts the electric signal to a pressure wave, that is received in another transducer (R) and converted into an electric signal. This signal is acquired with a sampling rate of 2 Gs/s, and with 8 bit resolution in a digital oscilloscope. The amount of noise is suppressed by averaging a large number of signals (100–1,000), and by making use of low-pass filters of 20 and 250 MHz. Also, in this way the resolution of the measurement is increased. A preamplifier with 31 dB gain in front of the oscilloscope amplifies the signal to a few millivolts, creating a maximum attenuation of approximately 110 dB for the complete measurement system. When the AWG sends the electric signal, a trigger signal is transmitted to the oscilloscope. In this way in every measurement the starting point $t = 0$, is determined. The measurement system is fully automated by a GPIB interface bus for transmission of the signals and signal acquisition in the oscilloscope. A representation of the setup is shown in Figure 7.

To cover the complete frequency range from 100 kHz–100 MHz, 8 pairs of broadband immersion transducers are used with center-frequencies of 200 kHz, 300 kHz, 800 kHz, 2.2 MHz, 5 MHz, 15 MHz, 50 MHz, and 80 MHz. These frequencies were selected in such a way that, for measurements away from the center-frequency of the transducers, a maximum of 6 dB additional attenuation is allowed.

Signal transmission

The combination of the AWG and the broad-band transducers allows for different types of output signals. A method of extracting the phase velocity and the attenuation is calculation of the fast-fourier transform (FFT) of a broad-band input signal, which was used in the work of Alig and Lellinger (1992). However, in this work for each frequency a narrow-band tone-burst was used, which was also applied with good results by Khatchikian et al. (1999). This method was applied, because the transmission of tone-bursts with different frequencies is very simple in the fully automated setup, and this technique is probably somewhat more accurate compared to determination of the phase velocity with FFT, with a broad-band input. The amplitude of the individual transmitted signals was adjusted to the efficiency of the transducers for a certain frequency, by

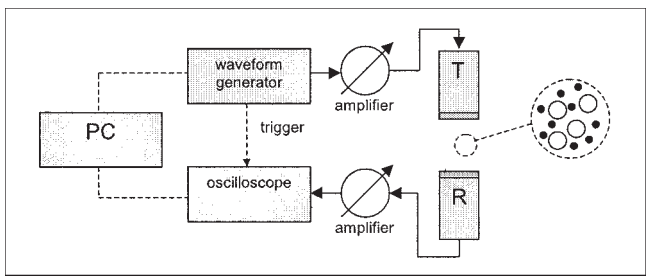

Figure 7. Representation of the setup.

transmitting the signal with an amplitude proportional to the inverse of the transducer characteristic. In this way better results were obtained at frequencies that are not close to the center frequency of the transducer.

Data analysis

To determine the velocity (c) and the attenuation coefficient (α), the received signal is compared in reference of a wave in a known fluid (for example, the continuous phase), which in this study will always be distilled water. Distilled water is used because all ultrasonic properties are well-known. In this way, the transfer function of the complete measurement system is not important, and only the excess properties of the dispersion compared to water are determined. The ultrasonic velocity and the attenuation coefficient in the dispersion are calculated, using

$$c = \frac{d}{t} = \frac{d}{d/c_w(T) + \Delta t} \tag{30}$$

$$\alpha = \frac{-\ln(I_2/I_1)}{d} + \alpha_w(T) \tag{31}$$

In these equations d is the path-length between the transducers. The ultrasonic velocity (c_w) and the attenuation coefficient (α_w) in water are temperature-dependent, and are determined by making use of well-established experimental values from Del Grosso and Mader (1972) and the *Handbook of Chemistry and Physics* (1994), respectively. The time difference (Δt) between the signal that has travelled through the dispersion, and the reference signal is determined by a cross-correlation of the two signals. This function is of the form

$$R_{xy}(\Delta t) = \sum_t x(t)\, y(t + \Delta t) \tag{32}$$

When two tone-bursts are compared, this function has a triangular shape and the time at which this function has its maximum represents the time difference between the two signals. An example is presented in Figure 8.

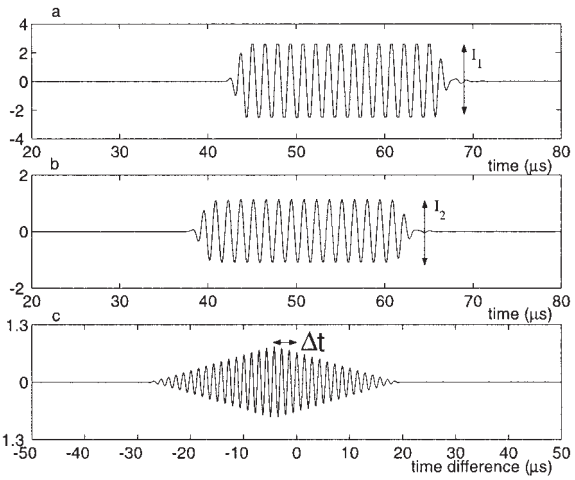

Figure 8. (a) signal in water, (b) signal in dispersion, (c) cross-correlation of signals a and b.

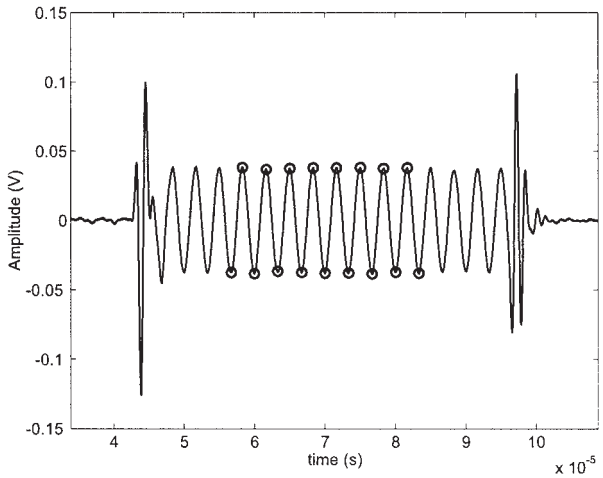

Figure 9. Distorted signal with large side maximums.

A tone-burst signal consists of a limited number of cycles, which implies that the signal is not completely narrow-banded, but has a certain frequency spectrum. Only in the limit of an infinite number of cycles (a continuous wave), the signal consists of one single frequency. The frequency spectrum broadens when the number of cycles decreases. The presence of other frequencies in the transmitted signal can give rise to problems, because these frequency components can travel with a different velocity, and can undergo less or more attenuation than the actual burst frequency. This can result in a received signal with heavily disturbed sides (Figure 9).

A drawback of these side effects is that they can lead to more than one maximum in the cross-correlation function, leading to uncertainty that the absolute maximum corresponds to the correct time delay. This can result in discontinuous velocity vs. frequency profiles, which is not possible from a physical point of view. To solve this problem, the method explained by Khatchikian et al. (1999) was adopted. These authors have shown that the presence of the distortions did not affect the position in time of the maximums, but only their height, which reduces the problem to finding the correct maximum from the different possibilities. From that point, it is possible to calculate the complete velocity profile starting from an undistorted measurement with low attenuation, assuming small differences in time delay with a small change in frequency.

The attenuation coefficient is easily calculated from an undistorted signal taking the peak-peak (maximum minus the minimum of the burst) value of the signals as shown by I_1 and I_2 in Figure 8. However, when the signals have large side maximums (as in Figure 9), this method gives erroneous values for the attenuation coefficient. To solve this problem, the average amplitude is determined from the middle 50% of the signal, as is shown by the open circles in Figure 9.

Gas holdup

For the independent measurement of the gas holdup using electrical conductivity, a probe containing two round stainless steel electrodes was used. A 1 kHz signal of 4-Volt was sent by the arbitrary waveform generator to the measurement probe

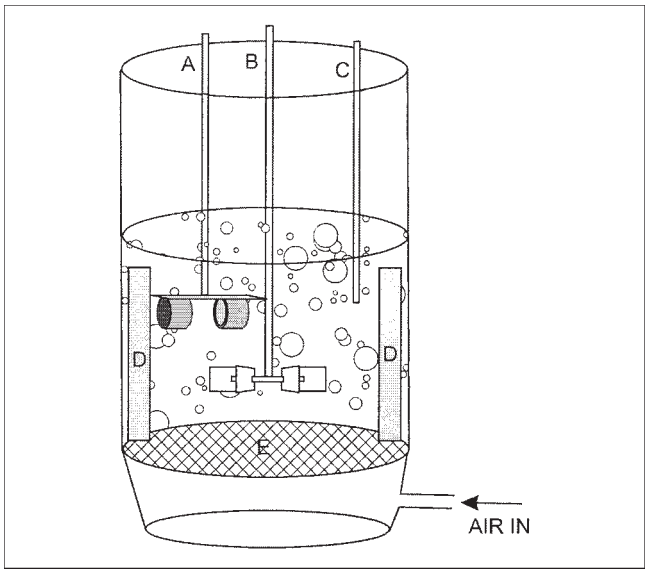

Figure 10. Stirred vessel.

(A)Transducer probe, (B) six-bladed Rushton turbine, (C) temperature sensor (PT-100), (D) baffles, and (E) porous plate.

and a reference resistance (6.75 kΩ) in series. From the measurement of the voltage over the reference resistance using the oscilloscope, it is possible to determine the resistance (and, consequently, the conductivity) of the medium between the stainless steel plates. The frequency of the used signal (1 kHz) was high enough to avoid polarization of the electrodes.

Experimental

Measurements of the ultrasonic velocity and the attenuation coefficient as a function of frequency in three-phase systems are new, and, to our knowledge, have never been published in literature. In order to develop the measuring technique, before applying it to a G-L-S system, first two-phase systems (S-L and G-L) were studied. The tank in which the G-L and the G-L-S measurements were performed is shown in Figure 10. Air was used as the dispersed gas phase, and deionized water as the continuous liquid.

The stirred vessel has an inner diameter of 15 cm and a height of 25 cm above the glass sintered porous plate. A six-bladed Rushton turbine with a diameter of 7.5 cm and four baffles assure equal dispersion of the particles. The temperature is controlled up to 0.1°C by a thermostatic bath, and measured with a PT-100 temperature sensor. The transducers are aligned in a probe with a variable distance with a maximum of 6 cm. To minimize the hydrodynamic influence of the size differences between the different transducer pairs, all the transducers are covered with a stainless steel jacket with equal outer dimensions. When a highly attenuating medium is used, this distance between the transducers can be as small as 1 mm. This distance should, of course, be much (say minimally 20x) larger than the size of the particles to ensure a representative sample between the transducers. Solid-liquid measurements were performed in a similar tank without the porous plate. A Plexiglas disc on top of the stirrer just below the surface prevented unwanted air induction into the liquid. Glass beads of 100–350 μm were used as the solid in S-L and G-L-S applications with the ultrasound method, and their size distribution was measured for comparison with a commercially available particle sizer (Microtrac X-100) using a laser scattering technique.

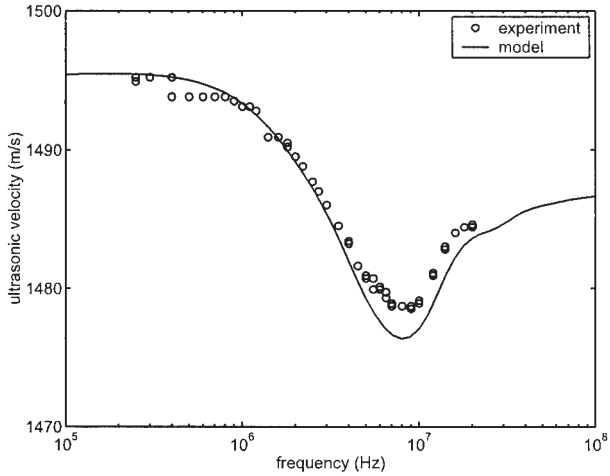

Figure 11. Ultrasonic velocity profile of 5% glass beads in water (S-L system).

The model line is the best fit through the experiments using a log-normal distribution.

Results and Discussion

S-L two-phase system

The results of measurements of the ultrasonic velocity and the attenuation coefficient in a system with glass beads of a known size distribution in water are presented in Figures 11 and 12.

The properties of the different compounds used in the model are listed in Table 1. The model line in Figure 11–12 was determined by using the mean, the variance, and the solid fraction as fit parameters in an optimization routine using the Nelder-Mead Simplex method (Nelder and Mead, 1965). The

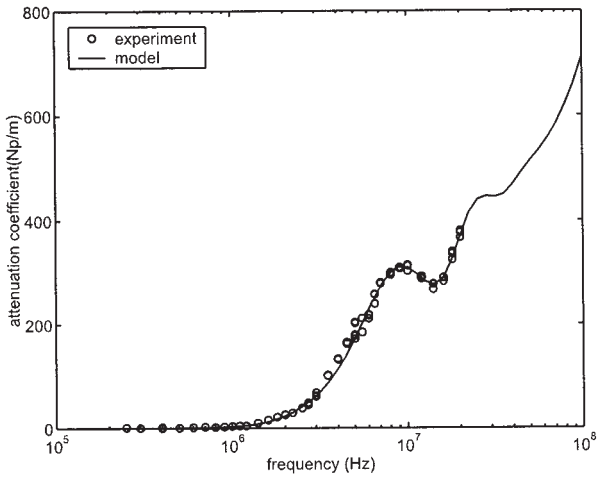

Figure 12. Attenuation coefficient profile of 5% glass beads in water (S-L system).

The model line is the best fit through the experiments using a log-normal distribution.

Table 1. Physical Properties of the Compounds Used in the Experimental and Theoretical Work at 21°C*

	Glass	Air	Hexadecane	Water
Density (kg m^{-3})	2500	1.2	769.3	998.0
Thermal conductivity (J m^{-1} s^{-1} K^{-1})	0.96	0.026	0.143	0.598
Specific heat (J kg^{-1} K^{-1})	$0.836 \cdot 10^3$	$1.007 \cdot 10^3$	$2.217 \cdot 10^3$	$4.18 \cdot 10^3$
Thermal expansion coefficient (K^{-1})	$3.2 \cdot 10^{-6}$	$3.4 \cdot 10^{-3}$	$8.15 \cdot 10^{-4}$	$2.04 \cdot 10^{-4}$
Attenuation coefficient per $freq^2$ (Np s^2 m^{-1})	$1 \cdot 10^{-13}$	$1.15 \cdot 10^{-11}$	$1.01 \cdot 10^{-13}$	$2.3 \cdot 10^{-14}$
Speed of sound (m s^{-1})	5200	344	1340	1485
Shear viscosity (kg m^{-1} s^{-2})	—	$1.8 \cdot 10^{-5}$	$3.34 \cdot 10^{-3}$	$0.98 \cdot 10^{-3}$
Shear rigidity (kg m^{-1} s^{-2})	$2.8 \cdot 10^{10}$	—	—	—
Speed of sound for spherical compressional waves in an elastic isotropic solid (m s^{-1})	3200	—	—	—

*The properties of air and water are taken from the Handbook of Chemistry and Physics (ed. Lide, 1994). The properties of glass are taken from the manufacturer or from Spelt et al. (1999). The properties of hexadecane (at 25°C) are taken from Herrmann and McClements (1999).

coefficient y in Eq. 23 was put 0.8 to normalize the two profiles on the basis of absolute values of the total velocity difference, and the total attenuation coefficient difference. The value of y ($0 < y < 0.9$) influenced the results only marginally as long as the attenuation coefficient profile was correctly taken into account. When only the velocity profile was taken into account (that is, $y=1$) in the optimization, the results were substantially different, and the general trend of the results obtained with both profiles was not followed. Perhaps, this could be overcome by considering a larger frequency region. The results are listed in Table 2. A comparison of the obtained particle-size distribution with the results obtained with the laser scattering technique is also listed in Table 2 and is visually represented in Figure 13.

The assumption of a log-normal distribution was reasonably good, as is shown in Figure 13. It should be mentioned that this assumption did not affect the mean, variance, and Sauter diameter when compared to a normal distribution. The results obtained with ultrasonic spectroscopy are in good agreement with the results obtained with the laser scattering technique, as can be seen from Table 2. The deviation in both Sauter and mean diameter is within 4%, which seems satisfactorily accurate. Also, the width of the distribution is predicted very well. The deviation between the measured solid holdup and the holdup based on the volume of glass in the reactor (noted with "in" in Table 2) is small. It seems that this can be attributed to local differences of solids holdup within the tank, however, this has to be validated at a later stage.

From Figure 11 and 12, it can be seen that, both for the attenuation coefficient as well as for the ultrasonic velocity, the experiments and the fitted model line are in good agreement. Measurements of the velocity profile in the region below 1 MHz were somewhat more laborious, because it was difficult to prevent air entrainment at the stirring speed used and, therefore, not a completely pure S-L system could be realized. The largest deviation between the model and the experiments is found in the frequency region 6–24 MHz, where the velocity deviates approximately 2 m/s from the experiments. A possible explanation for this could be that the actual profile of the volume fraction in the tank is changed because of a different distance between the transducers. The distance between transducers that transmit frequencies between 2.7 and 20 MHz was approximately 2 cm, and, between the other transducers, approximately 6 cm, because of the higher attenuation in the high-frequency region. This hypothesis, however, is not supported by the profile of the attenuation coefficient, which seems quite continuous. Also, the actual shape of the size distribution can influence the profile of the velocity, and could account for some deviation.

Table 2. Results of Ultrasonic Measurement of a 5% Dispersion of Glass Beads in Water in Comparison with Results Obtained by a Laser Scattering Technique

Glass Beads:	Ultrasound (S-L)	Ultrasound (G-L-S)	Laser Scattering
Mean (μ), μm	161	160	167
Variance (σ), μm	33	32	31
d_{32}, μm	175	173	179
Vol. fraction, %	5.5 (in 5.0)	6.1 (in 6.7)	—

G-L two-phase system

The results of measurements of the ultrasonic velocity, and the attenuation coefficient in a system with air bubbles in water are presented in Figures 14 and 15. The reactor was operated as a bubble column, so no stirring was applied during the experiments. The model lines in these figures were obtained from the optimization of the mean and variance of a log-normal distribution. The gas holdup was determined to be 5.8 vol. % by the conductivity measurement technique. In this nonturbulent gas-liquid system the measurement of the gas holdup using the conductivity technique could be compared with total liquid

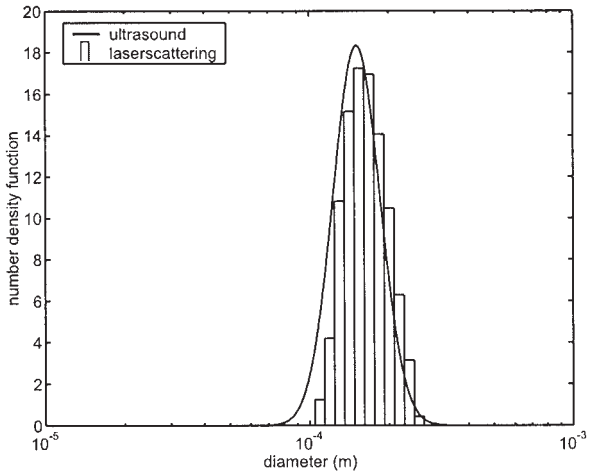

Figure 13. Comparison of ultrasound and laser scattering result for the glass beads particle-size distribution.

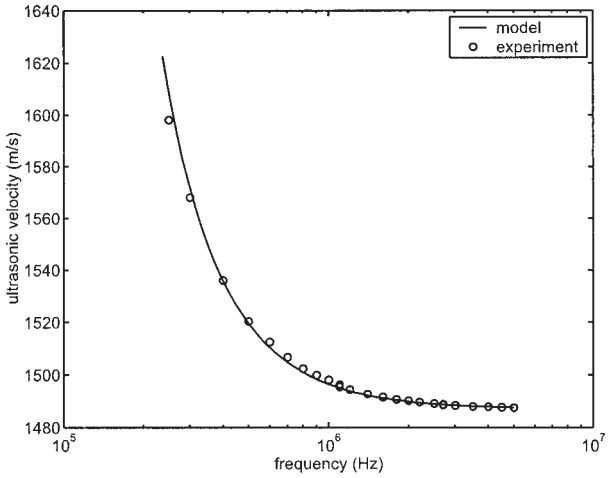

Figure 14. Ultrasonic velocity profile of 5.8% air bubbles in water (G-L system).

The model line is the best fit through the experiments using a log-normal distribution.

height reading in the reactor, and was found to be in good agreement. The gas holdup was determined from 7 readings (100 times averaged), with a standard deviation of 0.2 vol. % using a probe, which had exactly the same dimensions as the transducer probe in order to minimize differences in the tank hydrodynamics.

The mean and the variance of the bubble size distribution were 2.24 mm and 0.03 mm, respectively. The coefficient y in Eq. 23 was put to 0.5, because Δc and $\Delta\alpha$ are of the same order of magnitude. The absolute value of y did not influence the results to a large extent, which was expected from the very good agreement between the model and the experiments. The agreement between model and experiments is excellent in the velocity profile (Figure 14), but some irregularities can be observed in the attenuation coefficient profile (Figure 15), and also in the gas holdup from the conductivity measurements. The irregularities can be attributed to local differences in holdup and distribution in time, which can also be observed from the large time variation of the amplitude of the received signals through the dispersion. For this reason, time averaging of the signals during at least 5 min turned out to be necessary.

Both the mean and variance of the distribution show a very narrow shape of the size distribution, which was confirmed by visual observation of the dispersion in the vessel. However, the actual value of the variance of the distribution also depends on the value obtained for the gas holdup that is used in the model calculation. When, for instance, a gas holdup of 6.0% (mean (5.8%) + standard deviation (0.2%)) was used in the calculation, the mean and variance were 2.29 and 0.10 mm, respectively. This causes a difference of 3% in the Sauter diameter. An advantage of the technique is that the values of the calculated interfacial areas lie within 0.5% and can thus be determined very accurately, which was also shown by Stravs and Von Stockar (1985). These authors compared the interfacial area obtained using ultrasound with the interfacial area obtained with laser scattering with good results. This good agreement between the experiments and the ultrasonic scattering theory in G-L systems originates partly from the relatively high frequencies used. In this frequency regime thermal waves do not contribute significantly to the total absorption/scattering, which implies that scattering of the incoming wave is the dominant mechanism over others.

A minimization of the sum of squares between the model and the experiments without fixing the gas holdup resulted in a gas holdup of 5.85%, which supports the result obtained with the conductivity measurements. In order to test the technique for the measurement of bubble-size *distribution* more extensively, a comparison of ultrasonic spectroscopy with, for instance, a camera technique should be performed.

G-L-S three-phase system

The results of measurements of the ultrasonic velocity and the attenuation coefficient in a system with glass beads of a known size distribution in water in the presence of air bubbles are presented in Figures 16 and 17. The results show that a good agreement between the model and the experiments can be obtained using the properties of air, water, and glass from Table 1. In Table 2, the mean diameter and variance of the solid-phase fraction are presented. The values are in good agreement with the values when there are no bubbles present, which means that the technique can be used with a high accuracy in bubbly systems. The gas bubbles in this system are smaller (d_{32} = 1.67 mm) compared to the gas-liquid two-phase system, probably due to the high stirring intensity (550 rpm). The gas holdup was determined by the conductivity method, and was 3.3%. The value of the coefficient y was set to 0.5 and variation thereof did not influence the result.

Miscellaneous

- An advantage of the developed technique is that it can be operated completely noninvasively, for instance, in bubble columns, where the attenuation is not too high, which means that the transducers can be inserted in the walls of the column and, therefore, the flow pattern is not disturbed. In systems with small droplets or solid particles, the attenuation is higher in the frequency region that is needed for the determination of parti-

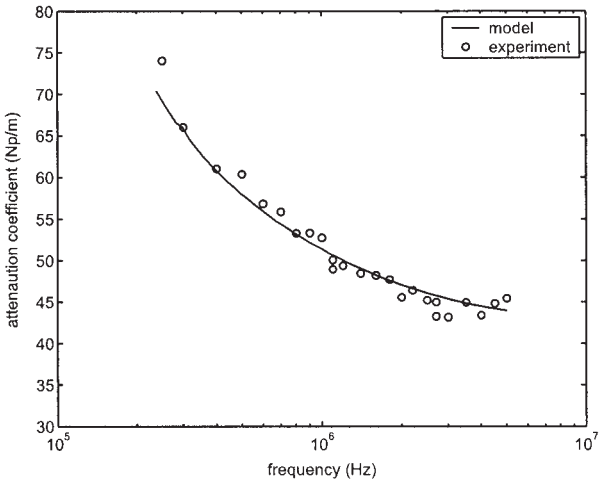

Figure 15. Attenuation coefficient profile of 5.8% air bubbles in water (G-L system).

The model line is the best fit through the experiments using a log-normal distribution.

cle size and smaller path lengths (for, instance, in a probe) are required.

- By making use of the tone-burst operating mode, the power input due to the ultrasonic waves can be set to any desired level. In this work, the average power input due to ultrasound was below 0.25 W (a transmitted signal frequency of 20 Hz was used), which avoids temperature differences between the transducers and the system and does not cause changes in the bubble distribution.
- The model that is used in this work assumes spherical particles, droplets and bubbles. In literature (Schaafsma and Hay, 1997) modifications of the theory are suggested to take different particle shapes into account.
- The influence of performing the measurements in the near-field of the transducers was studied using the tone-burst transmission method around an upward bubbly gas-flow with a certain, fixed diameter. The attenuation of the signal was not dependent on the path length between the transducers (with or without bubbly free zones in the near field of the transducers), which suggests that the influence is not significant. This is supported by the fact that the measurements in the solid-liquid system were performed at different measurement path lengths of the different transducer pairs that lead to continuous profiles of the attenuation coefficient and ultrasonic velocity.

Conclusions

In this work, a novel technique is developed for the *in situ* measurement of size distributions and phase holdup of particles, droplets and bubbles in two-phase, as well as in three-phase systems, respectively. It is shown that it is possible to resolve the size distribution of solid particles in the presence of gas bubbles and without. The results were compared with a commercial laser-scattering technique and were in good agreement.

For systems of gas bubbles in water, it was possible to describe the obtained experimental sound velocity and attenuation coefficient profiles accurately. The interfacial area could be determined very accurately from these measurements, but experimental validation of the bubble-size distributions obtained from these profiles should be performed using, for instance, a digital camera technique. From an overall perspective, it can be stated that this method is readily applicable in industrial applications for *in situ* determination of dispersed phase properties, which can be very important for design and control of chemical and physical processes.

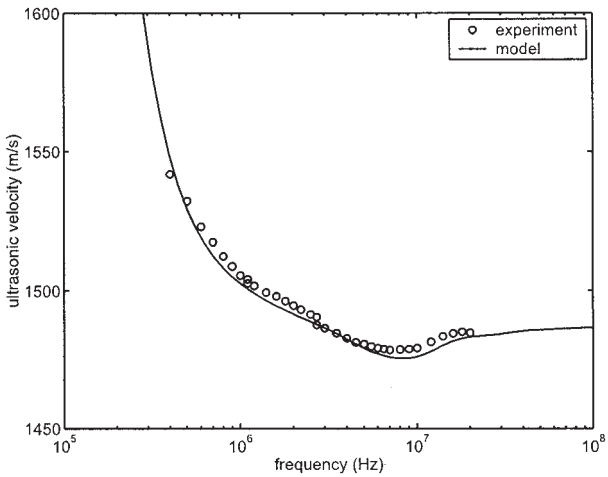

Figure 16. Ultrasonic velocity profile of a G-L-S system of 3.3% air bubbles and 6.1% glass beads in water.

The model line is the best fit through the experiments using log-normal distributions.

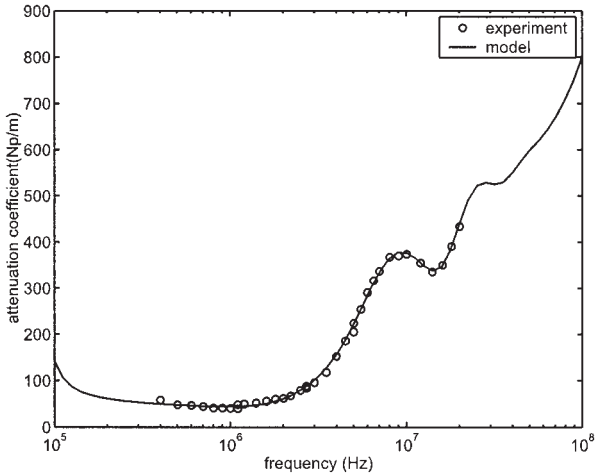

Figure 17. Attenuation coefficient profile of a G-L-S system of 3.3% air bubbles and 6.1% glass beads in water.

The model line is the best fit through the experiments using log-normal distributions.

Acknowledgment

The authors would like to acknowledge Benno Knaken for the technical support. Prof. A. Prosperetti is acknowledged for his contribution in the preparation of this manuscript. The Netherlands Organization for Scientific Research (NWO) is gratefully acknowledged for the financial support.

Notation

a = interfacial area, m^2/m^3
a_c, a_s, a_T = radius of particle times the wave number of the compressional, shear and thermal waves.
A, A_ε = cross-sectional area, m^2
$\boldsymbol{A}$ = shear wave potential, m^2
A_n, B_n, C_n = scattering coefficients
b_c,b_T = parameters defined in equations 8-9, K m^{-2}
c = adiabatic speed of sound, m s^{-1}
c_w = speed of sound in water, m s^{-1}
c_1 = speed of sound for spherical compressional wave in elastic isotropic fluid, m s^{-1}
C_p = specific heat, J kg^{-1} K^{-1}
d = path length, m
d_{32} = sauter diameter, m
f = frequency, s^{-1}
$f(0)$, $f(\pi)$ = far field scattering amplitudes, m
G, G_ε = conductivity, S
h_n = spherical Hankel functions of the first kind
i = imaginary unit ($\sqrt{-1}$)
I_1, I_2 = amplitudes in water, multiphase fluid, V
j_n = spherical Bessel functions
k_c, k_T, k_s = propagation constant of the compressional, thermal, and shear wave, m^{-1}
K = complex propagation constant, m^{-1}
L, L_ε = effective pathlength, m
M = parameter in log-normal distribution

n = order of spherical harmonics
N = number density of particles, m^{-3}
r = particle radius m
R = resistivity, Ω
S = parameter in log-normal distribution
t = time, s
y = coefficient in Eq. 23 m Np^{-1} or s m^{-1}
T = temperature, K

Greek letters

α = attenuation coefficient, Np m^{-1}
α_w = attenuation coefficient in water, Np m^{-1}
β = thermal expansion coefficient, K^{-1}
ε = dispersed phase fraction
γ = ratio of specific heats
η = viscosity, kg $m^{-1}s^{-1}$
λ = wave length, m
μ = mean particle size, m
μ = shear rigidity, kg $m^{-1}s^{-1}$
ν = kinematic viscosity$=\eta/\rho$, m^2 s^{-1}
ρ = density, kg m^{-3}
σ = standard deviation, m
σ = thermal diffusivity $= \tau/(\rho C_p)$, m^2 s^{-1}
τ = thermal conductivity, W m^{-1} K^{-1}
ϕ_c, ϕ_T = potential of compressional and thermal waves, m^2
ξ = tortuosity
ω = angular frequency, rad s^{-1}

Subscripts

1 = continuous phase
2 = dispersed phase
E = experimental
M = model
ε = dispersion

Literature Cited

Alig, I., and D. Lellinger, "Frequency Dependence of Ultrasonic Velocity and Attenuation in Two-Phase Composite Systems with Spherical Scatterers," *J. Appl. Phys.*, **72**, 5565 (1992).

Allegra, J. R., and S. A. Hawley, "Attenuation of Sound in Suspensions and Emulsions: Theory and Experiments," *J. Acoust. Soc. Am.*, **51**, 1545 (1972).

Bae, J. H., and L. L. Tavlarides, "Laser Capillary Spectrophotometry for Drop-Size Concentration Measurements," *AIChE J.*, **35**, 1073 (1989).

Barigou, M., and M. Greaves, "A Capillary Suction Probe for Bubble-Size Measurement," *Meas. Sci. Technol.*, **2**, 318 (1991).

Burgess, J. M., and P. H. Calderbank, "The Measurement of Bubble Parameters in Two-Phase Dispersions—I: The Development of an Improved Probe Technique," *Chem. Eng. Sci.*, **30**, 743 (1975).

Calderbank, P. H., "Physical Rate Processes in Industrial Fermentation. Part I: The Interfacial Area in Gas-Liquid Contacting with Mechanical Agitation," *Trans. Inst. Chem. Engrs*, **36**, 443 (1958).

Calderbank, P. H., F. Evans, and J. Rennie, "The Mass Transfer Efficiency of Distillation and Gas-Absorption Plate Columns. Part I: Techniques for Measuring Gas-Liquid Interfacial Areas and Foam Densities in Plate Columns," *Proc. of the Int. Symp. on Distillation,* Brighton, U.K., Inst. Chem. Engs., London, 51 (1960).

Calderbank, P. H., and J. Pereira., "The Prediction of Distillation Plate Efficiencies from Froth Properties," *Chem. Eng. Sci.*, **32**, 1427 (1977).

Cents, A. H. G., D. W. F. Brilman, and G. F. Versteeg, "Gas Absorption in an Agitated Gas-Liquid-Liquid System," *Chem. Eng. Sci.*, **56**, 1075 (2001).

Del Grosso, V. A., and C. W. Mader, "Speed of Sound in Pure Water," *J. Acoust. Soc. Am.*, **52**, 1442 (1972).

Duraiswami, R., S. Prabhukumar, and G. L. Chahine, "Bubble Counting using an Inverse Acoustic Scattering Method," *J. Acoust. Soc. Am.*, **104**, 2699 (1998).

Epstein, P .S., and R. R. Carhart, "The Absorption of Sound in Suspensions and Emulsions.* I. Water Fog in Air," *J.Acoust. Soc. Am.*, **25**, 553 (1953).

Foldy, L.L., "The multiple Scattering of Waves," *Phys. Rev.*, 67 107 (1945).

Gaunaurd, G. C., and H. Überall, "Resonance Theory of Bubbly Liquids," J. *Acoust. Soc. Am.*, **69**, 362 (1981).

Handbook of Chemistry and Physics, 75th ed. D. R. Lide, ed., CRC Press, Boca Raton, FL, (1994).

Herrmann, N., and D. J. McClements, "Ultrasonic Propagation in Highly Concentrated Oil-in-Water Emulsions." *Langmuir*, **15**, 7937(1999).

Khatchikian, P., U. Riebel, and U. Kräuter, "Phase Velocity of Ultrasound in Suspensions of Large Particles," *Acustica.*, **85**, 800 (1999).

Machon, V., A. W. Pacek and A. W. Nienow, " Bubble Sizes in Electrolyte and Alcohol Solutions in a Turbulent Stirred Vessel," *Trans. Inst. Chem. Eng.*, **75**, 339 (1997).

McClements, D. J., and P. Fairley, "Ultrasonic Pulse Reflectometer," *Ultrasonics*, **29**, 58 (1991).

McClements, D. J., "Principles of Ultrasonic Droplet Size Determination in Emulsions," *Langmuir*, **12**, 3454 (1996).

Medwin, H., "Counting Bubbles Acoustically: a Review," *Ultrasonics*, **14**, 7 (1977).

Nelder, J. A., and R. Mead, "A Simplex Method for Function Minimization," *Comp. J.,* **7**, 308 (1965).

Nishi, R. Y., "The Scattering and Absorption of Sound Waves by a Gas Bubble in a Viscous Liquid," *Acustica*, **33**, 65 (1975).

Pacek, A. W., I. P. T. Moore, A. W. Nienow, and R. V. Calabrese, "Video Technique for Measuring Dynamics of Liquid-Liquid Dispersion During Phase Inversion," *AIChE J.*, **40**, 1940 (1994).

Schaafsma, A. S., and A. E. Hay, "Attenuation in Suspensions of Irregularly Shaped Sediment Particles: A Two-Parameter Equivalent Spherical Scatterer Model," *J. Acoust. Soc. Am.*, **102**, 1485 (1997).

Spelt, P. D., M. A. Norato, A. S. Sangani, and L. L. Tavlarides, "Determination of Particle Size Distributions from Acoustic Wave Propagation Measurements," *Phys. Fluids*, **11**, 1065 (1999).

Stravs, A. A., and U. Von Stockar, "Measurement of Interfacial Areas in Gas-Liquid Dispersions by Ultrasonic Pulse Transmission," *Chem. Eng. Sci.*, **40**, 1169 (1985).

Stravs, A. A., A. Pittet, U. Von Stockar, and P. J. Reilly, "Measurement of Interfacial Areas Aerobic Fermentations by Ultrasonic Pulse Transmission," *Biotechnol. Bioeng.*, **28**, 1302 (1986).

Waterman, P. C., and R. Truell, "Multiple Scattering of Waves," *J. Math. Phys.*, **2** 512 (1961).

Weissberg, H. L. "Effective Diffusion Coefficient in Porous Media," *J. Appl. Phys.*, **34**, 2636 (1963).

Yianatos, J. B., A. R. Laplante, and J. A. Finch, "Estimation of Local Holdup in the Bubbling and Froth Zones of a Gas-Liquid Column," *Chem. Eng. Sci.*, **40**, 1965 (1985).

Yoshida, F., T. Yamane, and Y. Miyamoto, "Oxygen Absorption into Oil-in-Water Emulsions," *Ind. Eng. Chem. Process Des. Develop.,* **9**, 570 (1970).

Manuscript received July 7, 2003, and revision received Jan. 29, 2004.